



Journal of Mining and Environment (JME)
journal homepage: www.jme.shahroodut.ac.ir



Rock Fall Hazard Assessment using GeoRock 2D along Swat Motorway, Pakistan

Muhammad Adil*, Salim Raza and Ibrahim Amin

Department of Mining Engineering, University of Engineering and Technology, Peshawar, Khyber Pakhtunkhwa, Pakistan

Article Info

Received 27 February 2021

Received in Revised form 6 March 2021

Accepted 12 March 2021

Published online 12 March 2021

DOI: [10.22044/jme.2021.10599.2011](https://doi.org/10.22044/jme.2021.10599.2011)

Keywords

Rock Fall Simulation

Hazard Assessment

Highway

Slope Stability

Swat Motorway

Abstract

Despite the slope stability measures, rock falls are witnessed at section KM-37 of the Swat motorway (M-16), Khyber Pakhtunkhwa, Pakistan. The geotechnical data analysis of the site reveals that although the chances of plane/slope failures are reduced from 43% to 23% with the help of the existing design, still there are possibilities of rock fall at the sight, which has also been witnessed during the field visits. The rock fall hazards are assessed through field tests and simulation, and significant stabilization measures are suggested. The rock fall tests are conducted, and then using the data obtained, the rock fall simulation is carried out using GeoRock 2D®. From a combination of the kinematic analysis and rock fall simulation, the hazard level along the slope ranges from moderate to high. The reason for this is the increasing velocity of the falling boulder and the impact of energy at the bottom of the slope. This is an indication of the risk, as the most hazardous area is at the toe of the slope, where the highway road is the main element at risk. Rock boulders of different shapes and sizes are released from a couple of benches in order to check their impacts on the highway. Based on the simulation, it is concluded that the spherical shaped boulders are released from higher benches covering more horizontal distances and reaching the highway with a higher bouncing heights at the toe of the slope than the cylindrical shaped boulders. The maximum bounce height of 7 m has been recorded at the toe of the slope. In order to reduce the impacts of energy and bounce heights of the boulders striking the slope surface, certain mitigation measures are suggested like a ditch of a specific size filled with sand or fine debris at the toe of the slope. Draping wire mesh on the slope surface and a retaining wall or fence would be greatly helpful and economical to reduce the rock falling hazards along the road side at section KM-37 of the Swat motorway.

1. Introduction

Rock fall is the downward movement of rocks, debris and/or soil under the gravitational stresses, and is mainly due to cutting and blasting of rocks during the construction of roads or highways without a proper understanding of the geological and geotechnical investigations of the rock slopes [1]. Other driving factors include rain or seismic activity, which can cause loose rocks to fall. Throughout the history, these types of hazards have been experienced when human or nature disturbs the balance of natural or artificial rock slopes. These failures are classified on the basis of the type of downslope movement, i.e. slide, rotational or

flow. In order to identify the dangerous zones, conducting field work survey supported by aerial photographs, collecting history of rock fall events, and modelling the expected rock fall trajectories using STONE have been carried out [2].

In steep mountainous areas, rock fall, which is a frequent and fastest type of landslide, is common to occur. It is very favorable to occur in the rock strata that is highly jointed, weak, and weathered, having a high slope face angle [1]. According to Wiecezorek, in a case study of the recent failures from the Staircase Falls, the failure of the rock strata occurred due to the metrological conditions,

✉ Corresponding author: adil.m4726@gmail.com (M. Adil).

and in two cases, without knowing the triggers due to which the failures occurred. They evaluated the geological as well as the hydrological factors that contributed to the detachment of the strata. The factors that helped in causing the failures were hydrological conditions, discontinuities conditions and their orientation, lithology, and weathering [3].

Highways are vulnerable to rock falls wherever they cut across the mountains, plateaus, ridges or similar topographic features in the terrain areas. In the context of highway rock slopes, the potentially unstable slopes present hazards and pose risks to the traffic, to the transportation infrastructure, to the local economies, and to the environment, as shown in Figure 1.

Using different rating systems, usually rock fall hazard assessment is carried out. The rating

systems assign values of different weights of the falling rock boulders, existing geological conditions, weathering conditions, and other road characteristics [4]. Guzzetti and Reichenbach in order to determine the loss of velocity of the falling boulders at the impact points and friction angle of the rolling boulders, obtained by recoding a combination of the existing lithology and landslide inventory maps [5]. It is a very uncertain and complex phenomenon to know the impact of the rock fall. Depending on the mechanical properties of the slope material, mass, and velocity of the boulder and impact angle, it can vary from completely elastic to almost completely inelastic [6].



Figure 1. Unstable rock cut slope at KM-37 section of the Swat motorway.

The rockfall activities along the highways or motorways are not considered hazardous until the boulders enter the roadway. These type of activities become noticeable if the rockfall results in a damage in the infrastructure or loss of life. These events remain a threat for all the regulatory authorities who are responsible for providing safe and reliable highways in an economical fashion [7].

Keeping in view the potential hazards associated with rock falls and slope stability, the current

research work was conducted in order to evaluate the roadside conditions of the Swat motorway at section KM-37. This motorway is passing through mountains and ridges, cutting of which may cause a serious slopes failures and may cause problems in the flow of traffic. For this purpose, the field tests were conducted and the data was collected, on the basis of which simulation was done using the RocFall® software. RocFall® is a 2D modelling commercial software that has been designed to

analyze the rockfall hazard by simulating the behavior of the falling boulders along a used defined 2D cross-sectional profile by adopting a “hybrid” approach. It uses the lumped mass method to model the rockfall trajectories, and a rigid body approach to assess the striking impact of the boulder on the slope surface. In order to determine the loss of energy at the impact points while the boulder is rolling down the slope, RocFall requires values of coefficients of the normal and tangential restitutions. This software can determine the bouncing height of the falling boulder along the whole profile, downward velocity, associated energy, and stopping point of the boulder (called “rock end-points” in RocFall 2D) [8].

2. Location and general geology

Geologically, the Swat motorway project area lies in the Peshawar basin. Internally, the Peshawar basin comprises Quaternary sedimentary rocks that include fluvial deposits (gravels and sand), and lacustrine deposits. However, the outer fringes of the basin are predominantly fanglomerate derived from the adjacent encircling mountains such as the Malakand-Lower Swat Ranges in the north, the Attock-Cherat-Dara Adamkhel Ranges in the south, and the Khyber Ranges to the west [9].

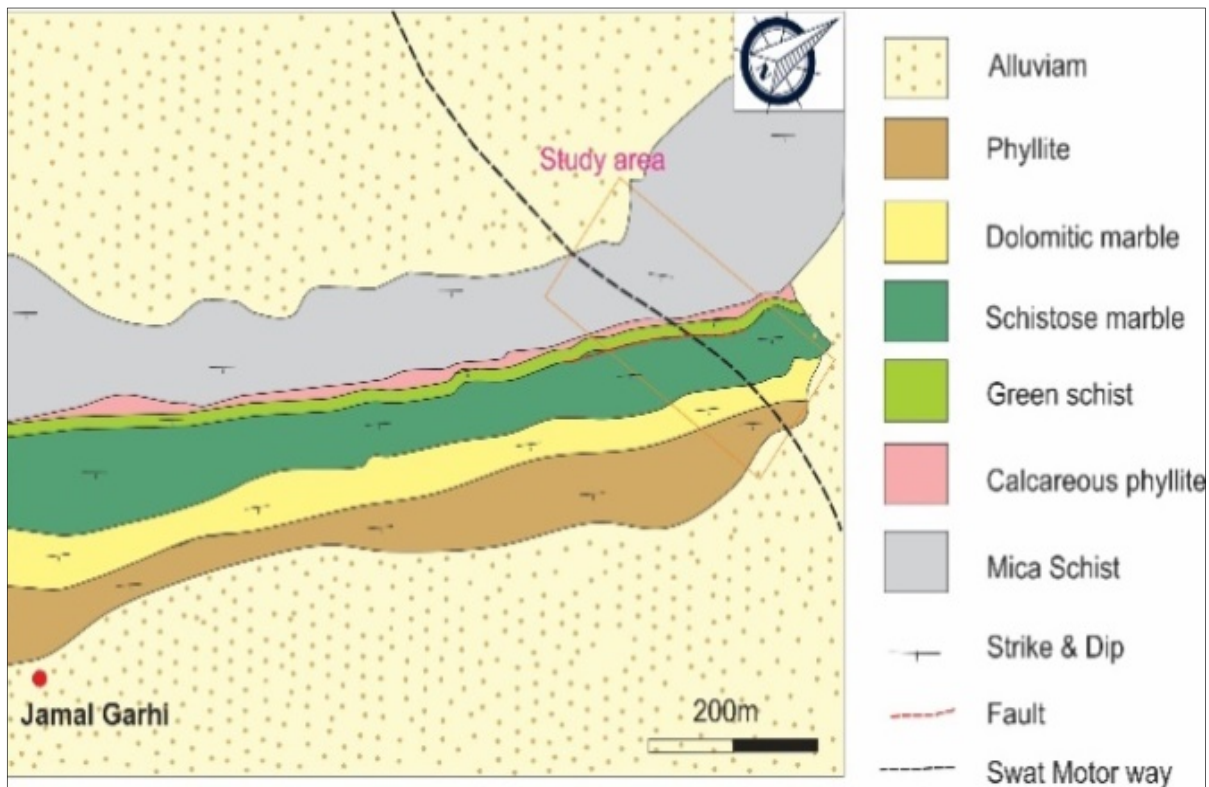


Figure 2. Geology of the studied area (KM-37) of the Swat motorway.

Sediments of the Peshawar basin have been impounded by the uplifting of the Attock-Cherat Range and movement on Main Boundary Thrust (MBT) located at its southern fringes [10, 11]. These rocks range in the age from the late Precambrian to the early Mesozoic (Figure 2).

3. Methodology

3.1. Field investigation

A reconnaissance field survey was conducted in order to observe the rock fall prone areas. It was

observed that the steep rock cut slopes constructed within the weak degraded rock masses were mostly unstable. Although several benches were made in the sloping face, still there are chances of rock failures, which can be seen in Figure 3. In order to assess the hazards of rock fall towards the highway, the real time field tests of rock fall were conducted by releasing rock boulders of different sizes from two different benches on the slope (Table 1) to see the effect of the rock fall.

Table 1. Results of real time rock fall tests at section KM-37.

Sr. No.	Shape	Mass (kg)	Height of releasing point	Max. horizontal distance
1	Cylindrical	50	50 m	40 m
2	Spherical	40	50 m	56 m
3	Spherical	40	40 m	68 m
4	Spherical	30	40 m	50 m

**Figure 3. Unstable rock cut slope prone to failure at KM-37 of the Swat motorway.**

The most critical section (left side, NE direction) of KM-37, where the rock slope is divided into five benches of about 12 m height and 3 m width each. At this location, the rock slope has 61 m total height and laid for 200 m along the beds striking NE and dip in the SE direction. The location of the unstable rocks are visually determined by observing one major fault along the joints in the cuts, as shown above in Figure 3.

3.2. Rock fall simulation analysis

The lumped mass method accompanied by GeoRock 2D software is used for the rock fall simulation, which is easily available and widely used in the simulation of rock fall problems. The lumped-mass simulation method considers the block's mass as a concentrated single point and simplifies the calculation models by ignoring the size and shape of the boulder [12].

This software can determine the rock fall trajectory, bounce height, pre-impact energy, velocity, and run-out distance of falling rocks. However, the collision of two bodies always results in the transfer and loss of energy, which depends up on the fundamental properties, i.e. the mass,

impact velocity, and environment in which the collision takes place [1].

According to Palma, B. *et al.* (2012), the GeoRock 2D software was used to determine the runout distance of the falling boulders and the energy lost at the impact points at the cliff. In order to perform the rockfall simulation using the GeoRock 2D, the following input parameters are required: (1) boulder's shape, size, weight, and starting velocity; (2) values of R_n and R_t that show the loss of energy at the striking points; and (3) values of the roughness co-efficient, used to model the loss of energy due to rolling. The output of the model includes the following: (1) type of downward movement of the boulder along the trajectory; (2) runout distance; and (3) energy of the block along the falling trajectory [13].

The GeoRock software uses the lumped mass method for analysis with the following assumptions:

1. Plan outline
2. Slope profile similar to a broken line consisting of straight line segments
3. Point boulder
4. Negligible air resistance [14]

The slope material properties, i.e. coefficient of normal restitution (Rn) and coefficient of tangential restitution (Rt), are pre-defined and reflect the post-impact rebounding velocity (Table 2). It is the relative velocity of a falling rock after the collision to initial velocity before collision. Its values are in the range of 0 to 1, i.e. if it is closer to 0, it means that the rock slope contains vegetation with a loose material like clay overburden or loose debris that shows that the falling rock material striking the slope material will rebound with zero velocity and thus the falling boulder will quickly stop. The values near to 1 represent hard rocks that rebound back with the same velocity with which strikes the slope [1].

Based on the particle analysis, using the lumped mass method, the rockfall trajectories were simulated along the 2D slope cross-section by considering the boulder as a particle with constant mass. This constant mass is used to calculate the highest kinetic energy that any rock boulder can attain while passing through each horizontal location along the section [15].

Table 2. Properties of slope material.

Nr.	Description	Rn	Rt
1	Solid rock	0.9	0.8
2	Degraded rock	0.7	0.7
3	Sand	0.4	0.6
4	Rock detritus	0.6	0.6
5	Fine debris	0.32	0.82
6	Debris with vegetation	0.29	0.8
7	Debris with shrubs	0.3	0.7
8	Terrain or grass	0.31	0.79
9	Paved surface	0.4	0.9

Characterization of the slope profile is very important because the condition of rocks in the slope and the number and orientation of

discontinuities can cause the falling rocks to behave like a projectile after striking the slope surface while falling downward. This can modify the trajectory formed by the falling boulders during the simulation or even increase the run out distance of the boulders [16].

The cut faces at KM-37 of the Swat motorway were thoroughly analyzed and it was determined that they were mainly composed of three types of materials, i.e. degraded rock (actual rock that was cut and slope was made), sand (fine material like fine debris or clay), and paved surface (highway road), as shown in Table 3. Each material has its own properties (R_n and R_t), as discussed earlier, due to which the impact of rock fall varies while striking these surfaces. A 2D cross-section of the rock slope is shown in Figure 4.

Table 3. Parameter values of slope material.

Slope Material Parameters			
Nr.	X(m)	Y (m)	Material
1	8.21	87.73	Degraded rock
2	10.21	85.73	Degraded rock
3	13.21	85.73	Degraded rock
4	16.21	80.73	Degraded rock
5	19.21	80.73	Degraded rock
6	24.21	70.73	Degraded rock
7	27.21	70.73	Degraded rock
8	32.21	60.73	Degraded rock
9	35.21	60.73	Degraded rock
10	40.21	50.73	Degraded rock
11	43.21	50.73	Degraded rock
12	48.21	40.73	Degraded rock
13	51.21	40.73	Degraded rock
14	56.21	30.73	Degraded rock
15	56.89	30.62	Sand
16	56.94	29.8	Sand
17	60.52	29.8	Sand
18	61.21	30.68	Paved surface
19	76.21	30.73	Paved surface

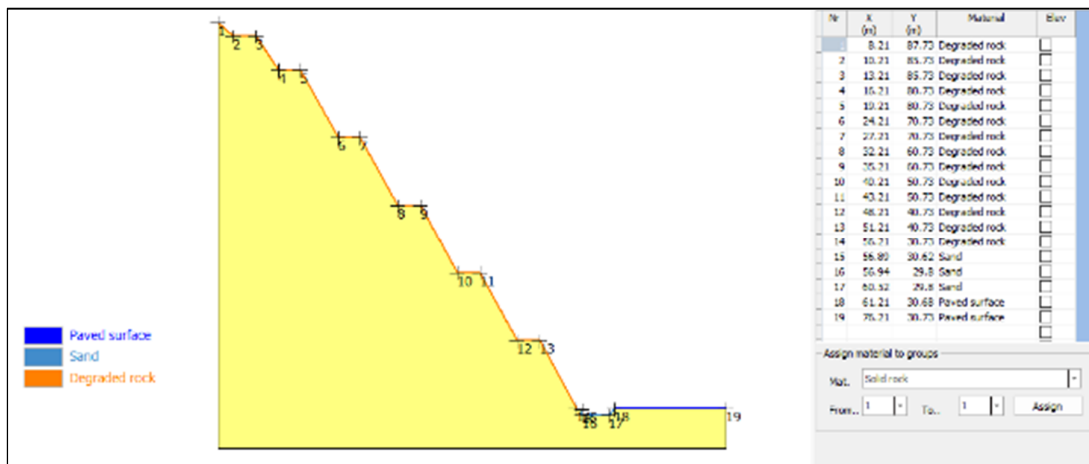


Figure 4. 2D cross-section of rock slope at KM-37 of Swat motorway.

4. Results and discussion

A total of 198 discontinuities were observed in the slope during the scanline survey including bedding, faults, joints, and cracks, as shown in Table 4. During the survey, dip and dip direction, persistence, type, aperture, spacing, infilling material, and smoothness of the surfaces of each discontinuity were recorded (Annexure I).

The Rocscience software (DIPS) was used in order to display the major planes along and across the cut slope to analyze the chances of plane failure using the data of dip and dip direction of all

discontinuities (Annexure II). The pole plot and contour plot of these discontinuities are shown in Figure 5. Analysis was carried out for Schist and Marble individually as well as combined as the rock slope at this section composing of Schist and Marble, as shown in Table 5.

Table 4. Dicontinuity data of rock slope at KM-37.

S. No.	Discontinuity type	No. of discontinuities
1	Bedding	23
2	Fault	1
3	Joint	149
4	Fissures (cracks)	25

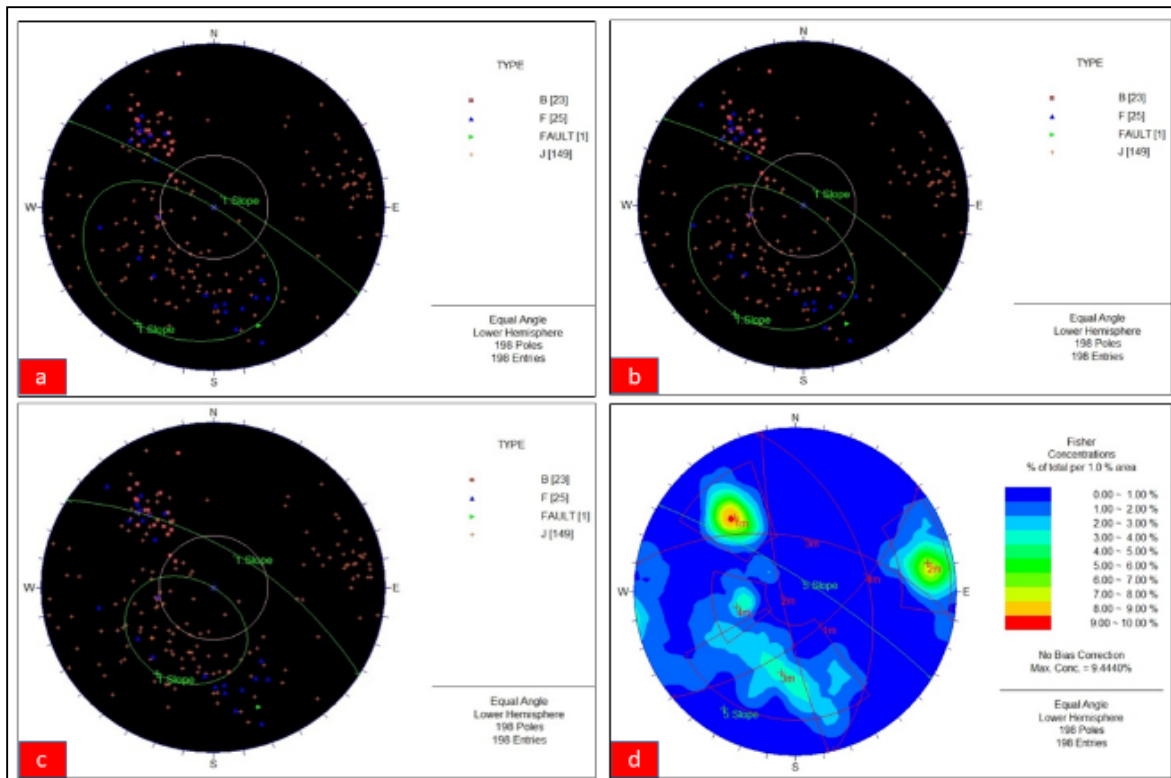


Figure 5. Pole plot for plane failure analysis at (a) site slope (b) 1:0.25 slope (c) 1:0.5 slope complete section of KM-37 and (d) contour plot with major planes-complete section of KM-37.

Table 5. Plane failure analysis of slope at KM-37 of Swat motorway.

Description	Plane failure probability (%)		
	Schist + Marble (%)	Schist (%)	Marble (%)
Site slope	43.00	52.00	34.34
1:0.25 (75.96 ⁰) slope	36.80	47.00	32.00
1:0.5 (63.43 ⁰) slope	23.00	19.00	19.19

4.1. Scenarios

The simulation was conducted without considering any restriction or barrier on the slope as per field investigation. The upper part of the slope comprised a highly jointed and weak rock mass. A ditch was designed at the toe of the slope

in order to prevent the falling boulders from entering into the highway.

The purpose of designing ditches or catchment benches is to collect the falling boulders or blocks at the toe of the slopes as it helps in absorbing the energy of the falling rocks. The significance of these ditches or trenches can be expressed by the

block catchment performance, which can be evaluated using the graphs obtained from the rockfall simulation [17].

A total of eight scenarios were created by varying the size, weight, shape, and releasing point of the boulder. Two release points were considered, one by releasing the boulders from the bench number five (approximately 50 m high) and the other from the bench number three having a height of around 30 m.

In general, the rocks in this area are metamorphic, and their elasticity is around

10125000 kilopascal (kPa) or 12.12 gigapascal's (GPa) and density of 2700 kg/m³. The values of the coefficient of normal restitution (Rn) and coefficient of tangential restitution (Rt) were taken as per Table 2. The other parameters like the boulder's shape, diameter, mass, and height were changed for each scenario in order to check the energy impact, moment of inertia, bounce height, and maximum horizontal distance covered by the falling rocks. Ten trajectories were drawn for each scenario. A summary of all the eight scenarios is shown in Table 6.

Table 6. Results of rockfall simulation for all eight scenarios.

Scenario No.	Boulder shape	Boulder mass (kg)	Release Height (m)	Moment of Inertia (kg m ²)	Max. pre-impact energy (kJ)	Max. bounce height (m)	Bounce height at the fence (m)	Max. velocity (m/s)	Max. distance covered (m)
1	Sphere	485	50	23.76	94.38	12	7.0	19.73	65.2
2	Cylindrical	424	50	29.24	107.2	11.7	2.4	22.49	45.3
3	Sphere	485	30	23.77	74.28	6.65	2.5	17.50	66.3
4	Cylindrical	424	30	29.24	60.5	6.5	3.2	16.89	60.7
5	Sphere	38	50	0.344	7.039	12	1.9	19.20	60.5
6	Cylindrical	42	50	0.99	8.0	12.13	6.4	19.42	68
7	Sphere	38	30	0.344	5.64	6.7	3.0	17.2	61.5
8	Cylindrical	42	30	0.99	6.30	12.01	7.0	17.24	66.5

4.2. Pre-impact energy

As a result of the simulation, 10 trajectories were drawn each time, which resulted in the production of energy graphs. As the slope is divided into benches, the falling rocks, therefore, bounce after striking the surface of the benches. Depending on the slope material, much of the pre-impact energy is lost after collision of the boulder with the slope surface, sometimes resulting in the fragmentation of the boulder as well.

The resulting graphs of all the scenarios are shown in Figure 6, in which the energy transformation is shown along the horizontal distance covered by the boulder. The analysis showed that the cylindrical-shaped boulder in scenario 2, when dropped from the higher point (i.e. 50 m) had a maximum pre-impact energy having the maximum moment of inertia while a lower runout distance. This is because the cylindrical-shaped boulder had a more effective area of friction due to which most of the time the motion begun with sliding, resulting in lowering after the impact energy and a lower runout distance.

At the slope, the average height of the bench is 12 m. The impact of energy increases whenever the rock boulder falls from a higher point to gain more energy without colliding with the slope surface. In scenario 1, the spherical-shaped boulder gained the 2nd most high pre-impact energy covering more

runout distance because of a round shape, which was less effective towards friction. In all the other scenarios, despite the change in mass of the boulder, the gain in energy is low, as either the mass of the boulder is less or the releasing point is lower.

4.3. Velocity

The slope consists of three types of materials, as discussed earlier. The velocity of the falling rock boulders depends on the type of downward motion and slope material.

The boulders sliding on the face of the slope will have a low velocity due to friction as compared to a boulder falling freely from the upper benches down to the road. It was observed during the field tests that the cylindrical-shaped boulders moved downward without sliding on the slope face, while the spherical-shaped boulders slid on the bench faces.

This was also validated by simulation of the rockfalls, as shown in the graphs (Figure 7). Due to the sliding motion of the spherical-shaped boulders, they experienced more friction, resulting in a low downward velocity, as compared to the cylindrical-shaped boulders. According to Table 6, all the cylindrical-shaped boulders had a high moment of inertia and a maximum downward velocity, as compared to the spherical-shaped boulders. However, depending on the other factors

like the impact energy, striking point, and bounce height, different boulders covered different horizontal run out distances. It was also observed that the heavier weighted cylindrical-shaped

boulders covered a less horizontal distance than the lighter cylindrical boulders, as compared to the spherical-shaped boulders when it they dropped down from the same release points.

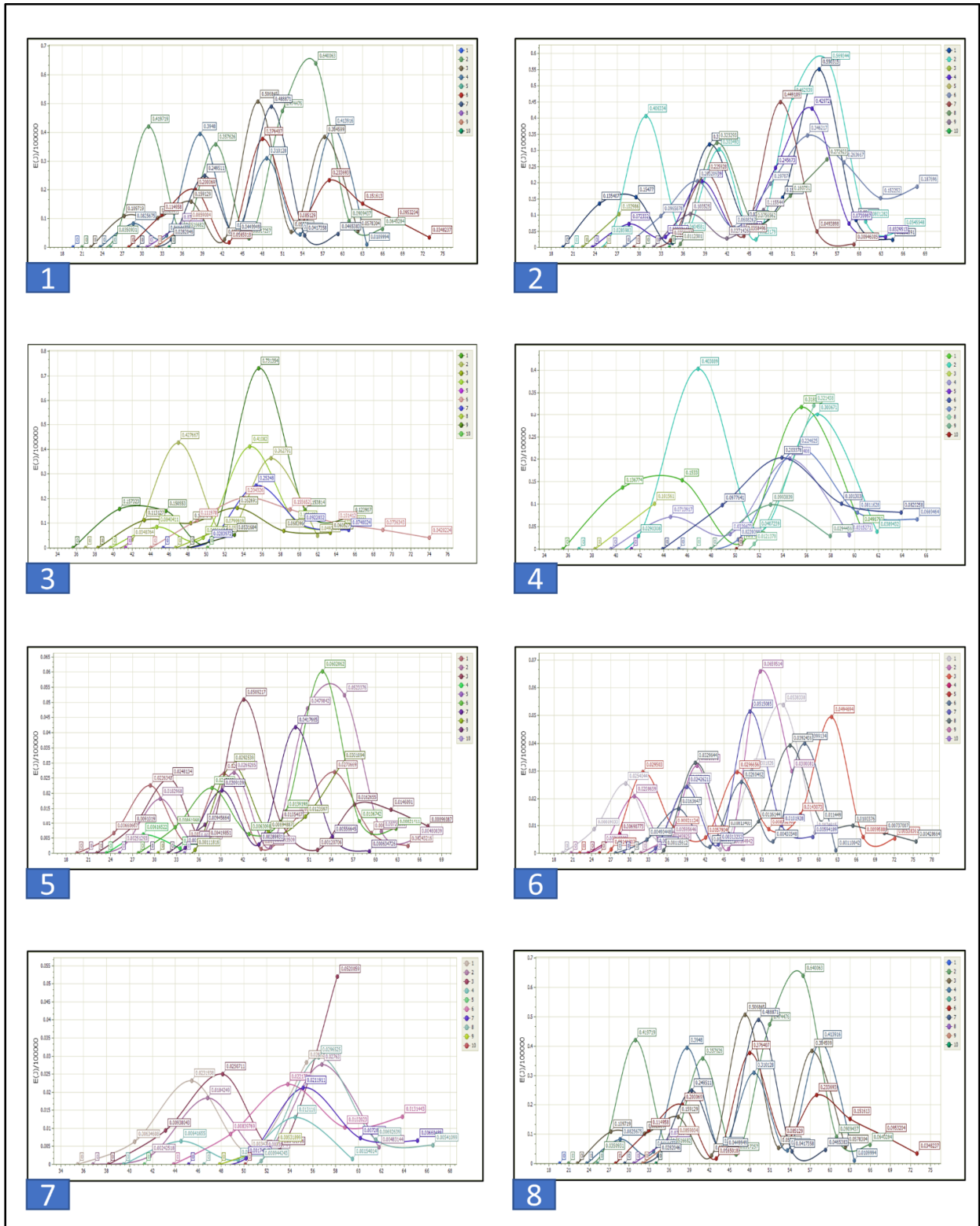


Figure 6. Graphs of energy for all eight scenarios.

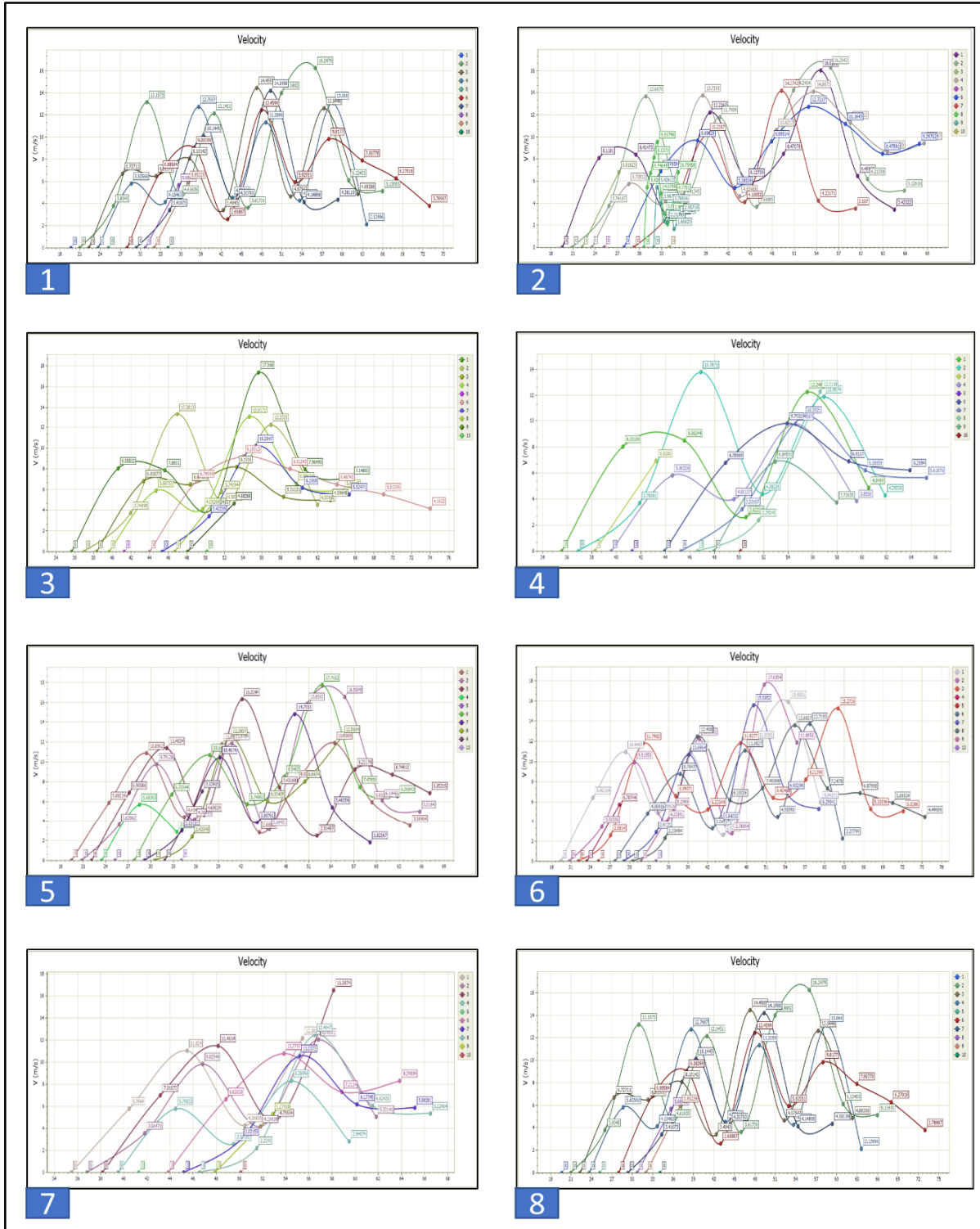


Figure 7. Graphs of velocity for all eight scenarios.

4.4. Bounce height

The bounce height trajectories show that the rock boulders from the releasing point show a less bounce in the initial stage, and as the boulder

moves downward striking the slope surface with an increasing velocity and in combination with the material properties of the benches with which the boulder collides, the bounce height increases up to 12 m.

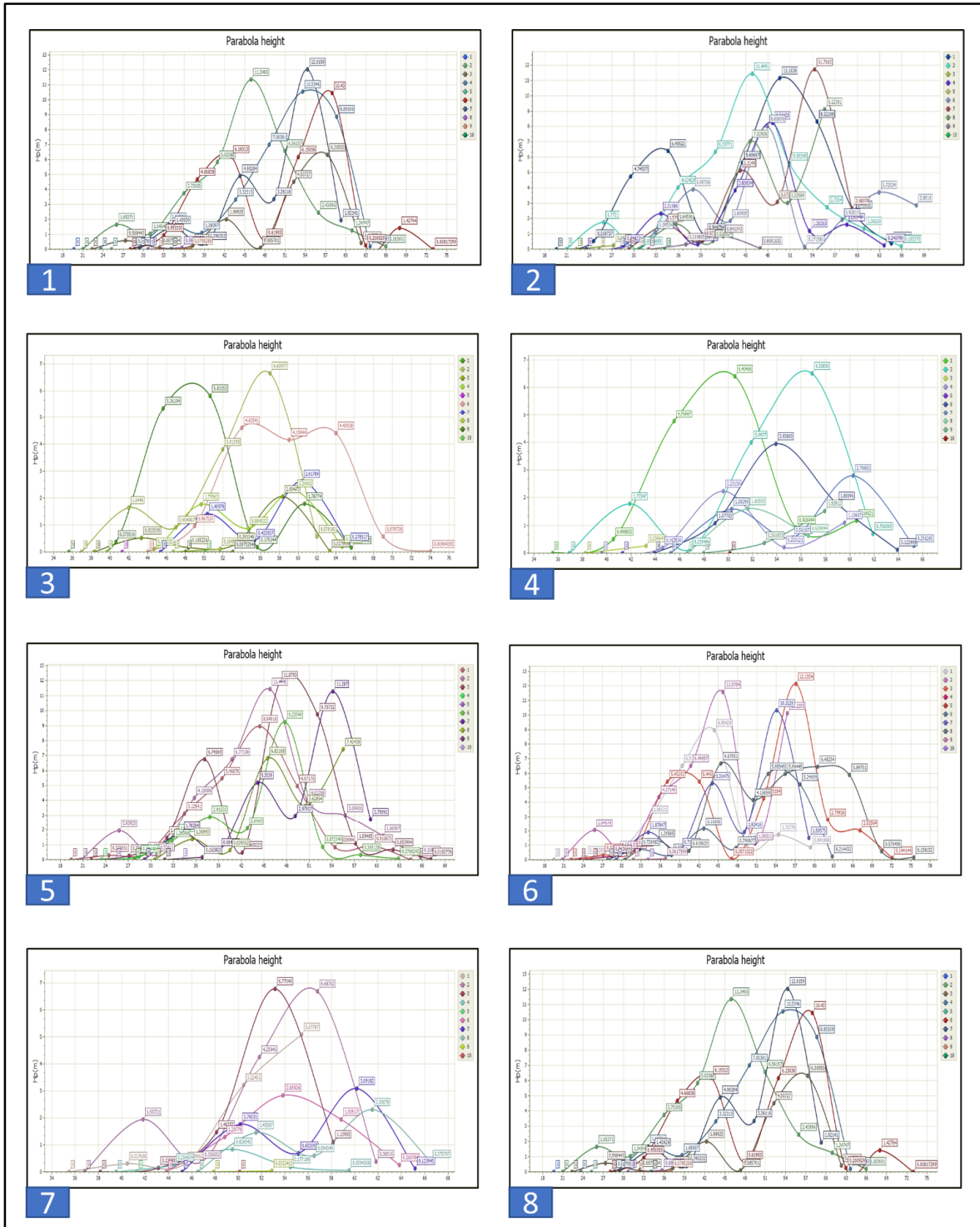


Figure 8. Graphs of bounce height for all eight scenarios.

This peak bounce was observed in most of the scenarios at around 45-55 m horizontal distance. However, we were more concerned with the bounce height at the toe of the slope near the road shoulder at 61 m abscissa, where the fence was to

be installed to stop the boulder from coming into the highway. The maximum bouncing height of 7 m at the road shoulder was observed in scenario 1 and scenario 8. The bounce height depends on the striking impact of the boulder with other material

surfaces. The values of coefficient of normal restitution (R_n) and coefficient of tangential restitution (R_t) were taken as per Table 2. These values are the reflection of the impact of the rock boulder bounce height after striking different surfaces. Depending on the type of downward motion of the rock boulder, the bounce height varies. Each bench has an average height of about 12 m. In case a rock boulder gets a chance to fall down freely without rolling or sliding over the surface experiences more bounce height, as compared to the one that slides on the slope surface and having a low velocity and a low pre-impact energy. Consequently, as observed in Table 6, in either case (scenario 1 or scenario 8), whether the rock boulder was spherical- or cylindrical-shaped, experienced the maximum bounce height, i.e. 7 m, at the fence location. The rock boulders having the maximum initial velocity and pre-impact energy will gain more bounce height, as shown in the following graphs (Figure 8) for all scenarios.

5. Conclusions

There are certain zones on the Swat motorway where the chances of land sliding are more. One of these locations is at the section of KM-37, where the rock is excavated and the height reaches 61 m. In the research work documented here, the rock fall hazard assessment was done through the field tests and simulation, and significant stabilization measures were suggested. According to the kinematic analysis, the planar failure was very likely to occur at KM-37 having failure chances of 43% (site slope), which was reduced to 23% by reducing the angle to 1:0.5, as shown in Table 5. From a combination of the kinematic analysis and rockfall simulation, the hazard level along the slope ranges from moderate to high. The reason for this is the increasing velocity of the falling boulder and the impact of energy at the bottom of the slope. This is an indication of the risk as the most hazardous area is at the toe of the slope, where the highway road is the main element at risk.

Boulders of different shapes and sizes were released from a couple of benches in order to check their impact on the road. Boulder weighings from 38 kg to 485 kg were considered for the rock fall simulation. A total of eight scenarios were created by changing the boulder weight, shape, and releasing point. Based on both the field tests and simulation, it was observed that the spherical-

shaped boulders released from higher benches, travelling long horizontal distances on the road, and reaching the highway with higher bounces at the toe of the slope, as compared to the cylindrical-shaped boulders. Except for scenario 2, in all the other scenarios, the rock boulders entered the highway with different bounce heights after striking the slope surface. The maximum bounce height for both the spherical- and cylindrical-shaped boulders at the toe of the slope was recorded as 7 m. This suggests that a retaining wall or fence is required in order to stop the boulders from entering the highway. The pre-impact energy ranges from 5.64 kJ to 107.2 kJ.

In order to reduce the impact of energy and bounce heights of the boulders, a ditch 4 m wide and 1 m deep was suggested to be designed at the toe since most of the boulders fell in the ditch area at the toe of the slope. The ditch is required to be filled with sand or fine debris due to the lower values of the tangential and normal restitutions. This would help in absorbing the kinetic energy of the free falling rock boulder, and will result in reduction of the bouncing heights.

Based on this work, it recommended to check the effect of changing the slope angle and width of the catchment benches along with the cost evaluation.

Conflict of interest

On behalf of all the authors, the corresponding author wishes to state that there is no conflict of interest.

Annexure I

S. No	Description	Remarks
RD 36 + 770 to 36 + 862		
	Persistence	1-20 m
	Aperture	Very narrow to tight
	Infilling	Surface stain, clay, Quartz
	Spacing	Moderate to close
	Roughness	Smooth, rough to slightly rough
	Water condition	Wet to dry
RD 36 + 904 to 37 + 200		
	Persistence	Moderate to high
	Aperture	Narrow to tight
	Infilling	Surface stain, clay, Quartz
	Spacing	Wide to close
	Roughness	Smooth, rough to slightly rough
	Water condition	Wet to dry

Annexure II

Scanline Survey Data for Section of KM 36-37 of Swat Motorway.
 F = Fissure, J = Joint, and B = Bedding

Sr. No.	Running distance	Dip	Dip direc	Discont. type	Lithology	Sr. No.	Running distance	Dip	Dip Direc	Discont. type	Lithology
1	36+770	44	145	F	Schist	114	37+006	85	86	J	Marble
2	36+772.7	45	145	F	Schist	115	37+006	80	325	J	Marble
3	36+772.7	72	10	J	Schist + Marble	116	37+011	50	275	J	Marble
4	36+772.7	60	8	J	Schist	117	37+011	70	248	J	Marble
5	36+776.4	37	140	F	Schist	118	37+011	19	120	J	Marble
6	36+776.4	78	231	J	Schist	119	37+015	75	325	B	Marble
7	36+784	55	160	F	Schist	120	37+016	40	278	J	Marble
8	36+784.3	63	2	J	Schist	121	37+016	82	222	J	Marble
9	36+784.3	65	335	J	Schist	122	37+016	39	250	J	Marble
10	36+786	40	2	J	Schist	123	37+016	32	195	J	Marble
11	36+786	61	30	J	Schist	124	37+018	69	320	B	Marble
12	36+786	50	34	J	Schist	125	37+023	65	58	J	Marble
13	36+790	33	285	B	Schist + Marble	126	37+023	28	265	J	Marble
14	36+798	52	300	B	Schist + Marble	127	37+023	88	100	J	Marble
15	36+800	86	210	J	Marble	128	37+024	84	86	J	Marble
16	36+803	70	175	J	Marble	129	37+025	55	262	J	Marble
17	36+804	45	301	B	Marble	130	37+028	28	298	J	Marble
18	36+804	58	255	J	Schist	131	37+028	50	230	J	Marble
19	36+804	89	160	J	Marble	132	37+028	85	83	J	Marble
20	36+807	76	152	J	Marble	133	37+028	55	190	J	Marble
21	36+808	80	66	J	Marble	134	37+028	70	320	B	Marble
22	36+813	71	280	B	Marble	135	37+031	68	260	F	Schist
23	36+817	65	311	B	Marble	136	37+031	48	250	J	Schist
24	36+819	71	155	F	Schist	137	37+032	74	170	F	Schist
25	36+821	85	35	J	Marble	138	37+032	65	316	B	Marble
26	36+823	61	316	B	Marble	139	37+035	70	75	J	Marble
27	36+823	60	311	J	Marble	140	37+037	45	198	J	Marble
28	36+827	75	321	B	Schist + Marble	141	37+037	40	220	J	Marble
29	36+831	66	305	J	Marble	142	37+037	65	318	F	Schist
30	36+831	49	212	J	Marble	143	37+039	64	68	J	Schist
31	36+831	70	160	J	Marble	144	37+040	75	70	J	Schist
32	36+836	86	255	J	Marble	145	37+045	65	165	F	Schist
33	36+836	88	260	J	Marble	146	37+045	80	85	J	Schist
34	36+838	55	170	B	Schist	147	37+046	48	195	J	Schist
35	36+838	90	60	J	Schist	148	37+046	75	81	J	Schist
36	36+840	54	176	J	Schist	149	37+048	62	179	F	Schist
37	36+841	26	311	J	Schist	150	37+051	80	66	J	Schist
38	36+845	40	195	J	Schist	151	37+051	56	235	F	Schist
39	36+846	79	230	J	Schist	152	37+058	82	286	J	Schist + Marble
40	36+846	50	229	J	Schist	153	37+058	45	321	B	Schist + Marble
41	36+850	65	311	J	Schist + Marble	154	37+058	54	318	B	Schist + Marble
42	36+850	83	45	J	Schist + Marble	155	37+062	70	230	J	Schist + Marble
43	36+850	70	178	J	Schist + Marble	156	37+064	18	300	J	Schist + Marble
44	36+854	80	58	J	Schist + Marble	157	37+064	65	316	F	Schist + Marble
45	36+856	55	330	B	Schist + Marble	158	37+064	63	245	J	Schist

Continuous of Scanline Survey Data for Section of KM 36-37 of Swat Motorway.
 F = Fissure, J = Joint, and B = Bedding

46	36 + 856	76	75	J	Schist + Marble	159	37 + 064	54	310	J	Schist
47	36 + 856	67	211	J	Schist + Marble	160	37 + 065	66	200	J	Schist
48	36 + 856	56	356	J	Schist + Marble	161	37 + 066	66	324	J	Schist
49	36 + 857	55	185	J	Marble	162	37 + 068	65	72	J	Schist
50	36 + 857	66	330	J	Marble	163	37 + 074	68	319	F	Schist
51	36 + 857	62	305	J	Marble	164	37 + 076	87	266	J	Schist
52	36 + 857	30	215	J	Marble	165	37 + 078	60	320	F	Schist
53	36 + 857	81	275	J	Marble	166	37 + 081	38	260	J	Schist
54	36 + 857	34	252	J	Marble	167	37 + 084	34	265	J	Schist
55	36 + 857	80	60	J	Marble	168	37 + 085	85	335	J	Schist
56	36 + 857	77	80	J	Marble	169	37 + 088	55	98	J	Schist
57	36 + 861	85	81	J	Schist	170	37 + 088	80	75	J	Schist
58	36 + 862	65	174	F	Schist	171	37 + 088	63	320	B	Schist
59	36 + 904	56	185	F	Schist	172	37 + 089	78	86	J	Schist + Marble
60	36 + 904	57	75	J	Schist	173	37 + 091	84	77	J	Schist + Marble
61	36 + 904	76	275	J	Schist	174	37 + 091	55	322	B	Schist + Marble
62	36 + 905	50	330	J	Schist	175	37 + 091	80	80	J	Schist + Marble
63	36 + 913	61	174	F	Schist	176	37 + 095	56	328	F	Schist + Marble
64	36 + 913	45	235	J	Schist	177	37 + 098	45	200	J	Marble
65	36 + 914	57	220	F	Schist	178	37 + 098	15	240	J	Marble
66	36 + 915	75	168	J	Schist + Marble	179	37 + 102	60	320	B	Marble
67	36 + 919	80	166	J	Schist + Marble	180	37 + 102	75	160	F	Marble
68	36 + 921	20	157	J	Schist + Marble	181	37 + 118	82	161	F	Coal
69	36 + 924	65	180	J	Schist	182	37 + 118	62	156	F	Schist
70	36 + 924	38	251	J	Schist	183	37 + 118	63	328	J	Schist
71	36 + 926	66	78	J	Marble	184	37 + 119	52	240	J	Schist
72	36 + 927	36	260	F	Marble	185	37 + 119	55	148	F	Schist
73	36 + 933	66	332	B	Marble	186	37 + 127	60	245	J	Schist
74	36 + 935	46	325	B	Marble	187	37+127	50	216	J	Schist
75	36 + 936	70	38	J	Marble	188	37+130	80	346	B	Schist
76	36 + 936	66	40	J	Marble	189	37+130	45	184	J	Schist
77	36 + 938	59	220	J	Marble	190	37+130	82	315	F	Schist
78	36 + 938	58	246	J	Marble	191	37+131	53	238	J	Schist
79	36 + 938	50	258	J	Marble	192	37+131	45	136	J	Schist
80	36 + 944	55	200	J	Marble	193	37+131	76	80	J	Schist
81	36 + 944	50	210	J	Marble	194	37+135	63	235	J	Schist
82	36 + 947	35	308	B	Marble	195	37+135	65	310	F	Schist
83	36 + 947	37	258	J	Marble	196	37+141	68	230	J	Schist + Marble
84	36 + 947	40	225	J	Marble	197	37+147	66	205	J	Schist + Marble
85	36 + 948	55	315	J	Marble	198	37+147	54	318	B	Schist + Marble
86	36 + 959	45	218	J	Marble	199	37+148	45	170	J	Schist + Marble
87	36 + 964	82	102	J	Marble	200	37+149	64	316	J	Schist
88	36 + 964	50	322	B	Marble	201	37+149	78	235	J	Marble
89	36 + 966	55	200	J	Marble	202	37+151	83	78	J	Marble
90	36 + 970	79	80	J	Marble	203	37+151	65	204	J	Marble
91	36 + 971	30	306	B	Marble	204	37+153	50	328	B	Marble
92	36 + 973	77	90	J	Marble	205	37+157	80	258	J	Marble
93	36 + 975	50	203	J	Marble	206	37+157	68	116	J	Marble
94	36 + 975	62	335	J	Marble	207	37+157	35	221	J	Coal
95	36 + 978	52	190	J	Marble	208	37+157	65	150	F	Schist
96	36 + 980	50	160	J	Marble	209	37+160	60	311	B	Schist
97	36 + 985	88	240	J	Marble	210	37+160	70	145	J	Schist

Continuous of Scanline Survey Data for Section of KM 36-37 of Swat Motorway.

F = Fissure, J = Joint, and B = Bedding

98	36 + 985	68	315	J	Marble	211	37+171	60	320	F	Schist
99	36 + 987	58	148	J	Marble	212	37+172	66	140	J	Schist
100	36 + 992	53	186	J	Marble	213	37+177	84	138	J	Schist
101	36 + 993	30	285	J	Marble	214	37+178	35	205	J	Schist
102	36 + 994	46	286	J	Marble	215	37+181	65	178	J	Schist
103	36 + 998	88	260	J	Marble	216	37+182	75	200	J	Schist
104	36 + 998	60	145	J	Marble	217	37+184	62	321	B	Schist
105	36 + 998	55	180	J	Marble	218	37+185	48	145	J	Schist
106	37 + 001	82	245	J	Marble	219	37+185	52	98	J	Schist
107	37 + 001	48	152	J	Marble	220	37+191	48	311	F	Schist
108	37 + 001	60	315	F	Schist + Marble	221	37+191	60	158	J	Schist
109	37 + 001	35	265	J	Schist + Marble	222	37+191	40	285	J	Schist
110	37 + 006	70	323	F	Marble	223	37+194	78	86	J	Schist
111	37 + 006	18	308	J	Marble	224	37+194	61	195	J	Schist
112	37 + 006	84	71	J	Marble	225	37+194	55	322	B	Schist
						226	37+201	82	77	J	Schist

References

- [1]. Sazid, M. (2019). Analysis of rockfall hazards along NH-15: A case study of Al-Hada road. *International Journal of Geo-Engineering*, 10 (1): 1-13.
- [2]. Katz, O., Reichenbach, P. and Guzzetti, F. (2011). Rock fall hazard along the railway corridor to Jerusalem, Israel, in the Soreq and Refaim valleys. *Natural Hazards*, 56 (3): 649-665.
- [3]. Wieczorek, G.F., Stock, G.M., Reichenbach, P., Snyder, J.B., Borchers, J.W. and Godt, J.W. (2008). Investigation and hazard assessment of the 2003 and 2007 Staircase Falls rock falls, Yosemite National Park, California, USA. *Natural Hazards and Earth System Sciences*, 8 (3): 421-432.
- [4]. Regmi, A. D., Cui, P., Dhital, M. R., & Zou, Q. (2016). Rock fall hazard and risk assessment along Araniko Highway, Central Nepal Himalaya. *Environmental Earth Sciences*, 75 (14): 1-20.
- [5]. Guzzetti, F., Reichenbach, P. and Wieczorek, G.F. (2003). Rockfall hazard and risk assessment in the Yosemite Valley, California, USA. *Natural Hazards and Earth System Sciences*, 3 (6): 491-503.
- [6]. F. Guzzetti et al., "STONE : a computer program for the 3D simulation of rock-falls \$," Vol. 28, pp. 1079–1093, 2002.
- [7]. Youssef, A.M. and Maerz, N. H. (2009). Slope stability hazard assessment and mitigation methodology along eastern desert Aswan-Cairo highway, Egypt. *Earth Sciences*, 20(2).
- [8]. Tagliavini, F., Reichenbach, P., Maragna, D., Guzzetti, F. and Pasuto, A. (2009). Comparison of 2-D and 3-D computer models for the M. Salta rock fall, Vajont Valley, northern Italy. *Geoinformatica*, 13(3), 323-337.
- [9]. Khaliq, A.H., Waseem, M., Khan, S., Ahmed, W. and Khan, M.A. (2019). Probabilistic seismic hazard assessment of Peshawar District, Pakistan. *Journal of Earth System Science*, 128(1), 1-22.
- [10]. F. Report, 4 4.1 Geology and Tectonics, No. March. 1998.
- [11]. M.Q.J.A.H. Kazmi, "Geology Tectonics of Pakistan."
- [12]. San, N.E., Topal, T. and Akin, M.K. (2020). Rockfall Hazard Assessment Around Ankara Citadel (Turkey) Using Rockfall Analyses and Hazard Rating System. *Geotechnical and Geological Engineering*, 1-21.
- [13]. Palma, B., Parise, M., Reichenbach, P. and Guzzetti, F. (2012). Rockfall hazard assessment along a road in the Sorrento Peninsula, Campania, southern Italy. *Natural Hazards*, 61 (1): 187-201.
- [14]. R. Mass, S. Analysis, and G. Hoek-brown, "Data Input / Output: Hoek-Brown Input and Output Parameters."
- [15]. Mineo, S., Pappalardo, G., Mangiameli, M., Campolo, S. and Mussumeci, G. (2018). Rockfall analysis for preliminary hazard assessment of the cliff of Taormina Saracen Castle (Sicily). *Sustainability*, 10 (2): 417.
- [16]. Costa Silveira, L. R. and Lana, M.S. (2018). Rockfall Hazard Assessment Approach for Slopes in a Quartzite Mine. In *ISRM VIII Brazilian Symposium on Rock Mechanics-SBMR 2018*. International Society for Rock Mechanics and Rock Engineering.
- [17]. Akin, M., Dinçer, İ., Ok, A. Ö., Orhan, A., Akin, M. K. and Topal, T. (2021). Assessment of the effectiveness of a rockfall ditch through 3-D probabilistic rockfall simulations and automated image processing. *Engineering Geology*, 283, 106001.

ارزیابی خطر سقوط سنگ با استفاده از GeoRock 2D در امتداد بزرگراه Swat، پاکستان

محمد عادل^{۱*}، سلیم رضا^۱ و ابراهیم امین^۱

دانشگاه مهندسی و فناوری پیشاور، پیشاور، پاکستان

ارسال ۲۰۲۱/۰۲/۲۷، پذیرش ۲۰۲۱/۰۳/۱۲

* نویسنده مسئول مکاتبات: adil.m4726@gmail.com

چکیده:

با وجود اقدامات پایداری شیب، ریزش سنگ در قطعه KM-37 بزرگراه سوات (M-16)، خیبر پختونخوا، پاکستان مشاهده می‌شود. تجزیه و تحلیل داده‌های ژئوتکنیکی سایت نشان می‌دهد اگرچه احتمال شکست صفحه/شیب با کمک طرح موجود از ۴۳ به ۲۳ کاهش می‌یابد، اما با این وجود احتمال سقوط سنگ وجود دارد، که در بازدیدهای میدانی مشاهده شده است. خطرات سقوط سنگ از طریق آزمایشات میدانی و شبیه‌سازی ارزیابی شده و اقدامات پایداری قابل توجهی پیشنهاد می‌شود. آزمایش‌های سقوط سنگ انجام شد و سپس با استفاده از داده‌های بدست آمده، شبیه‌سازی سقوط سنگ با استفاده از GeoRock 2D صورت گرفت. با استفاده از ترکیبی از آنالیز حرکتی و شبیه‌سازی ریزش سنگ، سطح خطر در امتداد شیب از متوسط تا زیاد متغیر است. دلیل این امر افزایش سرعت سقوط تخته سنگ و تأثیر انرژی در پایین شیب است. این نشانه خطر است، زیرا خطرناکترین منطقه در بالاترین نقطه شیب قرار دارد، جایی که بزرگراه عنصر اصلی است که در معرض خطر است. برای بررسی تأثیرات آنها در بزرگراه، تخته سنگهای دارای اشکال و اندازه‌های مختلف از چند محدوده آزاد می‌شوند. بر اساس شبیه‌سازی، تخته سنگ‌های کروی شکل از ترازهای بالاتر آزاد می‌شوند که فواصل افقی بیشتری را پوشش می‌دهند و از ترازهای بالاتری نسبت به تخته سنگ‌های استوانه‌ای شکل به بزرگراه می‌رسند. حداکثر ارتفاع پرش ۷ متر در بالای شیب ثبت شده است. به منظور کاهش تأثیرات انرژی و ارتفاع سقوط تخته سنگ‌هایی که به سطح شیب برخورد می‌کنند، اقدامات کاهش خاصی مانند کانال یا تراشه به اندازه خاص که مملو از ماسه یا بقایای ریز در شیب دامنه است پیشنهاد می‌شود. نصب مش فلزی بر روی سطح شیب و دیوار حائل یا حصار برای کاهش خطرات ریزش سنگ در امتداد جاده در بخش KM-37 بزرگراه سوات بسیار مفید و مقرون به صرفه است.

کلمات کلیدی: شبیه‌سازی سقوط سنگ، ارزیابی خطر، بزرگراه، ثبات شیب، بزرگراه Swat.